



A novel natural image noise level estimation based on flat patches and local statistics

Zhuang Fang^{1,2} · Xuming Yi¹

Received: 28 February 2018 / Revised: 19 December 2018 / Accepted: 26 December 2018 /
Published online: 7 January 2019
© Springer Science+Business Media, LLC, part of Springer Nature 2019

Abstract

This paper proposes a high-precision algorithm for noise level estimation. Different from existing algorithms, we present a new noise level estimation algorithm by linearly combining the overestimated and underestimated results using combinatorial coefficients that can be tailored to the problem at hand. The algorithm has two distinct features: it avoids the underestimation of noise level estimation algorithms that employ the minimum eigenvalue and demonstrates higher accuracy and robustness for a large range of visual content and noise conditions. The experimental results that are obtained in this study demonstrate that the proposed algorithm is effective for various scenes with various noise levels. The software release of the proposed algorithm is available online at <https://ww2.mathworks.cn/matlabcentral/fileexchange/64519-natural-image-noise-level-estimation-based-on-flat-patches-and-local-statistics>.

Keywords Noise level estimation · Flat patches · Gaussian noise · Eigenvalue · Covariance matrix

1 Introduction

The noise level is a crucial parameter for many image processing algorithms and applications, such as image denoising [2, 6, 11, 33], segmentation [1, 28, 31], superresolution [8, 20] and image quality assessment [14]. The noise level is not always available in practice; however, it is often assumed to be known in many algorithms [2, 7, 9, 30, 32]. Thus, accurate and reliable noise level estimation for image processing is currently in high demand.

✉ Xuming Yi
xmyi.math@whu.edu.cn

Zhuang Fang
wdfangzhuang@163.com

¹ School of Mathematics and Statistics, Wuhan University, Wuhan, 430072, Hubei, People's Republic of China

² School of Science, Hubei University for Nationalities, Enshi, 445000, Hubei, People's Republic of China

The model of a noisy image is often expressed as $\mathbf{y} = \mathbf{x} + \mathbf{v}$. Here, $\mathbf{y} \in \mathbb{R}^{m \times n}$ is a measurement image, $\mathbf{x} \in \mathbb{R}^{m \times n}$ is a noise-free image, and $\mathbf{v} \in \mathbb{R}^{m \times n}$ is added white Gaussian noise with zero mean and variance σ^2 . The main objective of noise level estimation is to estimate the unknown variance σ^2 . Over the past decades, many noise level estimation algorithms have been proposed. These algorithms can be broadly divided into filter- [10, 13, 21, 22, 29] and path-based approaches [5, 12, 15, 16, 18, 19, 24, 34].

In filter-based methods, the noisy image is initially filtered by a low-pass filter. Then, the variance is estimated from the difference between the measurement image and its filtered image. The main challenge in these methods is to design suitable filters. Filter-based methods can also be applied in a transform domain, such as the discrete wavelet transform (DWT). Donoho [10] has proposed a method for estimating σ that depends only on the median absolute deviation of the wavelet coefficients at the finest scale. However, it is difficult to prove theoretically whether the result that is estimated via wavelet-based techniques is overestimated or not because the wavelet transformation has difficulty completely separating the image signal from a noisy image that contains complicated structures, edges, and high-frequency components. Oyet et al. [22] and Hashemi et al. [13] pointed out that the algorithm proposed in [10] may be inconsistent with the actual noise variance. Therefore, this estimation result is often used as an initial noise variance to improve the accuracy of noise level estimation [12, 17].

Patch-based methods play an important role in noise level estimation. In these methods, a noisy image is initially decomposed into a group of patches. Then, the flat patches are selected via various statistical techniques [5, 15, 16, 18]. Typically, patch-based methods estimate the noise level based on the minimal eigenvalue of the covariance matrix of the flat patches [15, 19, 24]. Based on the results that were obtained by Blom et al. [25, 26], Chen et al. [5] proved that both WT [19] and PCA [24] may underestimate the noise level. Hence, they proposed a new nonparametric algorithm for efficient noise level estimation. Unlike WT and PCA, wherein the noise level is estimated directly by the minimal eigenvalue, Jiang et al. [15] proposed an algorithm for estimating the noise level by the ratio of the minimal eigenvalue to a constant that is less than one. However, they did not determine whether the estimation results that were obtained by their algorithm were overestimated or not. Additionally, the algorithms [15, 19, 24] did not analyze the effect of the total number of flat patches on the estimation result. This study mainly focuses on solving the above-mentioned problems. Using Blom's theory, we establish the relationship between the eigenvalues of the covariance matrix of flat patches and the true noise variance. Based on this relationship, an overestimated result is obtained. Then, by combining the two noise level estimation results, namely, the underestimated and overestimated results, we propose a new noise level estimation algorithm.

The main contributions of this paper are as follows. First, based on Blom's theorem, the effects of the eigenvalues on the final estimation result were analyzed. The conditions for assessing whether an estimate was overestimated or not were presented. Second, a new noise level estimation algorithm was proposed. Moreover, we proved that the estimate that was obtained via the proposed algorithm is a linear combination of the overestimated and underestimated results and that the combinatorial coefficients are related to the number of flat patches. The results of extensive tests demonstrated that our algorithm can realize high performance in most cases, particularly for images that have high noise levels.

The remainder of this paper is organized as follows: Section 2 introduces the principles of that are used to select the weak textured patches and flat patches. An analysis of the basic theory is presented, and the proposed noise level estimation algorithm is described in Section 3. Section 4 specifies the parameter settings, presents the experimental results of

a computer simulation that utilized the proposed algorithm, and compares the results with those that were obtained via various other algorithms. The conclusions and a future research direction are discussed in Section 5.

2 Related studies

In this section, we review the weak textured patch selection and flat patch selection methods, which are foundational to this study.

2.1 Weak textured patch selection method

Image structure can be measured effectively by the gradient covariance matrix [33]. Accordingly, Liu et al. [19] developed a weak textured patch selection method. In their study, a noisy image was initially filtered by the horizontal derivative operators, which are denoted by \mathbf{D}_h , and the vertical derivative operators, which are denoted by \mathbf{D}_v . Then, the filtered image was decomposed into overlapping patches, which are denoted as $\bar{\mathbf{y}}_j$ that are of size $w \times w$. The top-left corner positions of all patches were obtained from the set $\{1, 2, \dots, m - w + 1\} \times \{1, 2, \dots, n - w + 1\}$. Subsequently, they were rearranged into vectors of $N = w^2$ elements. The total number of patches is denoted by s , and expressed as $s = (m - w + 1) \times (n - w + 1)$. Finally, an iterative weak textured patch selection algorithm and a noise level estimation algorithm were proposed. In the k^{th} iteration, the threshold, which is denoted as τ , is updated with a significance level δ and noise level σ_k as follows:

$$\tau = \sigma_k^2 F^{-1}\left(\delta, \frac{N}{2}, \frac{2}{N} \text{tr}(\mathbf{D}_h^T \mathbf{D}_h + \mathbf{D}_v^T \mathbf{D}_v)\right), \quad (1)$$

where $F^{-1}(\delta, \alpha, \beta)$ is the inverse gamma cumulative distribution function.

The weak textured patches that are extracted from the noisy images are denoted by \mathbf{p}_i . The covariance matrix $\sum_{\mathbf{p}}$ of the selected weak textured patches is defined as follows:

$$\sum_{\mathbf{p}} = \frac{1}{s'} \sum_{j=1}^{s'} (\mathbf{p}_j - \boldsymbol{\mu})(\mathbf{p}_j - \boldsymbol{\mu})^T, \quad (2)$$

where $\boldsymbol{\mu} = \frac{1}{s'} \sum_{j=1}^{s'} \mathbf{p}_j$, and s' is the total number of selected patches. According to the algorithm reported in [19], the noise level can be estimated as follows:

$$\sigma_w^2 = \min_{1 \leq i \leq N} (e_i), \quad (3)$$

where e_i represents the eigenvalues of $\sum_{\mathbf{p}}$.

2.2 Flat patch selection method

In the flat patch selection algorithm, the noisy image is decomposed into overlapping patches. Let $P = \{\mathbf{y}_l; l = 1, 2, \dots, s\}$ be the set of all patches from the noisy image \mathbf{y} , where \mathbf{y}_l is the observed patch, which has a patch size of $w \times w$. The average pixel intensity in patch \mathbf{y}_l is denoted by μ . Then, the local variance is defined by

$$\sigma_l^2 = \sum_{y \in \mathbf{y}_l} (y - \mu)^2 / (w^2 - 1). \quad (4)$$

For all flat patches, it follows that $(w^2 - 1)\sigma_l^2/\sigma^2 \sim \chi^2(r)(r = w^2 - 1)$, where $\chi^2(r)$ is a chi-square distribution with r degrees of freedom. Thus, $\sigma_l^2 \sim \gamma(r/2, 2\sigma^2/r)$ with the following probability density function (PDF):

$$f(x) = \begin{cases} \frac{1}{\Gamma(r/2)} x^{\frac{r}{2}-1} (\frac{r}{2\sigma^2})^{\frac{r}{2}} e^{-\frac{r}{2\sigma^2}x}, & x \geq 0, \\ 0, & \text{otherwise.} \end{cases} \tag{5}$$

The mean of σ_l^2 is as follows:

$$E(\sigma_l^2) = \frac{r}{2} \times \frac{2\sigma^2}{r}. \tag{6}$$

For the flat patches, the following theorem applies:

Theorem 1 [15] *There must exist a unique $\tilde{\sigma}^2(\tilde{\sigma} > 0)$ such that the following equations hold:*

$$\tilde{\sigma}^2 = E(\sigma_l^2 | \sigma_l^2 < \lambda \tilde{\sigma}^2), \tag{7}$$

and

$$\tilde{\sigma}^2 = \rho \sigma^2, \tag{8}$$

with

$$\rho = \frac{\int_0^{F^{-1}(\delta, \frac{r}{2}, \frac{2}{r})} xz(x)dx}{\int_0^{F^{-1}(\delta, \frac{r}{2}, \frac{2}{r})} z(x)dx}, \tag{9}$$

$$\lambda = F^{-1}(\delta, \frac{r}{2}, \frac{2}{r})/\rho, \tag{10}$$

where $z(x) = \sigma^2 f(\sigma^2 x)$ represents the PDF of $\gamma(\frac{r}{2}, \frac{2}{r})$, $F^{-1}(\cdot)$ is the inverse Gamma cumulative distribution function with $\frac{r}{2}$ shape parameter and $\frac{2}{r}$ scale parameter; and δ , which is a specified significance level, denotes the probability that the local variance is does not exceed $\lambda \tilde{\sigma}^2$, i.e., $P(\sigma_l^2 \leq \lambda \tilde{\sigma}^2) = \delta$ ($P(\cdot)$ represents the probability).

By employing Theorem 1, Jiang et al. developed an algorithm [15] for selecting flat patches. The main parameters and their interrelations are presented in Table 1. More details regarding the parameter settings and the experiment can be found in [15]. Next, the covariance matrix \sum_I that is generated from those flat patches is defined by

$$\sum_I = \begin{cases} \frac{1}{num_v - 1} (I - I_m^1)(I - I_m^1)^T, & num_v \geq w^2, \\ \frac{1}{r - 1} (I - I_m^2)(I - I_m^2)^T, & num_v < w^2, \end{cases} \tag{11}$$

where $I = \{\mathbf{y}_{l_1}, \mathbf{y}_{l_2}, \dots, \mathbf{y}_{l_{num_v}}\}$ is an $N \times num_v$ matrix and I_m^1 and I_m^2 are the column averages of I and I^T , respectively, where I^T is the transpose of I . According to the algorithm that is presented in [15], the noise level of the image is estimated as follows:

$$\hat{\sigma} = \frac{\bar{\sigma}_f}{\sqrt{\rho}}, \tag{12}$$

where $\bar{\sigma}_f$ satisfies the following equation:

$$\bar{\sigma}_f^2 = \min_{1 \leq i \leq N} (e_i), \tag{13}$$

in which e_i denotes the i^{th} eigenvalue of \sum_I .

Table 1 Different λ and ρ according to δ

δ	$w = 5$		$w = 6$		$w = 7$		$w = 8$		$w = 9$	
	λ	ρ								
0.7	1.3267	0.8510	1.2657	0.8772	1.2240	0.8956	1.1937	0.9091	1.1707	0.9196
0.8	1.3807	0.8918	1.3098	0.9113	1.2613	0.9248	1.2260	0.9348	1.1992	0.9424
0.9	1.4758	0.9372	1.3868	0.9489	1.3261	0.9569	1.2818	0.9627	1.2482	0.9672

3 Main results and algorithm

In this section, the theoretical foundation of the algorithm is discussed and the relationship between the eigenvalues and the noise level is analyzed. Then, we propose a new noise level estimation algorithm that is based on the flat patches and local statistics.

3.1 Eigenvalue analysis

To compute σ_w^2 in (3) and σ_f^2 in (13), we need the eigenvalues of the covariance matrix. Regarding the distribution of the covariance matrix eigenvalues, Chen et al. [5] proved the following theorem, which is crucial to this study.

Theorem 2 *Given a set of random variables $\{y_t[i]\}_{i=1}^s$, with each element following Gaussian distribution $N(0, \sigma^2)$ independently, the distribution of the noise estimates $\hat{\sigma}_t^2 = \frac{1}{s} \sum_{i=1}^s y_t[i]^2$ converges to the distribution $N(\sigma^2, \frac{2\sigma^4}{s})$ as s becomes sufficiently large.*

Let $\Phi(x) = \frac{1}{\sqrt{2\pi}} \int_{-\infty}^x e^{-t^2/2} dt$ denote the cumulative distribution function of a standard Gaussian distribution. Blom [25, 26] proved the following theorem.

Theorem 3 *Given n independent random variables, namely, x_1, x_2, \dots, x_N , that are generated from the normal distribution $N(\sigma^2, \nu^2)$ with order $x_1 \geq x_2 \geq \dots \geq x_N$, then, the expected value of x_i can be approximated by $\mathbb{E}(x_i) \approx \sigma^2 + \Phi^{-1}(\frac{N-\alpha+1-i}{N-2\alpha+1})\nu$ with $\alpha = 0.375$.*

Corollary 3.1 *If $i > \frac{N+1}{2}$, then $\mathbb{E}(x_i) < \sigma^2$. If $i < \frac{N+1}{2}$, then $\mathbb{E}(x_i) > \sigma^2$.*

Proof If $i > \frac{N+1}{2}$, then $N + 1 - 2i < 0$. By adding $N - 2\alpha + 1$ to both sides, we obtain $2N - 2\alpha + 2 - 2i < N - 2\alpha + 1$, that is, $\frac{N-\alpha+1-i}{N-2\alpha+1} < \frac{1}{2}$. Then, we have $\Phi^{-1}(\frac{N-\alpha+1-i}{N-2\alpha+1}) < 0$.

Let $i = N$. We obtain $\sigma^2 + \Phi^{-1}(\frac{1-\alpha}{N-2\alpha+1})\nu < \sigma^2$, with $\nu = \sqrt{\frac{2\sigma^4}{s}}$. □

The same method can be used to analyze the case of $i < \frac{N+1}{2}$.

Corollary 3.2 *The estimate of σ_w^2 in (3) satisfies the following equation:*

$$\sigma_w^2 = \sigma^2 + \Phi^{-1}\left(\frac{1 - \alpha}{N - 2\alpha + 1}\right)\nu < \sigma^2. \tag{14}$$

Proof In (3), the minimum eigenvalue is selected as the noise level. From Theorem 3, it follows that $i = N$. Then, the following relationship holds:

$$\mathbb{E}(x_N) \approx \sigma_w^2 = \sigma^2 + \Phi^{-1}\left(\frac{1 - \alpha}{N - 2\alpha + 1}\right)\nu < \sigma^2. \tag{15}$$

The smallest eigenvalue is smaller than the noise level when the number of redundant dimensions is larger than one. This completes the proof. □

Lemma 3.1 *Suppose the following relationship holds:*

$$\sigma_\rho^2 = \frac{\sigma^2 + \sqrt{\frac{2\sigma^4}{s}} \Phi^{-1}\left(\frac{N-\alpha+1-i}{N-2\alpha+1}\right)}{\rho}. \tag{16}$$

If $i < \frac{N+1}{2}$, then $\sigma_\rho^2 > \sigma^2$.

Proof Using the second mean value theorem for integrals, we prove that $0 < \rho < 1$, for all $\delta, r \in R$. Then, for $i < \frac{N+1}{2}$, $\rho < 1$ and $\sigma_\rho^2 = \frac{\mathbb{E}(x_i)}{\rho}$, we obtain $\sigma_\rho^2 = \frac{\sigma^2 + \sqrt{\frac{2\sigma^4}{s}} \Phi^{-1}(\frac{N-\alpha+1-i}{N-2\alpha+1})}{\rho} > \sigma^2$ from Corollary 3.1. □

Lemma 3.2 If $\frac{N+1}{2} \leq i \leq N - \alpha + 1 - \Phi((\rho - 1)\sqrt{\frac{s}{2}})(N - 2\alpha + 1)$, then $\sigma_\rho^2 > \sigma^2$.

Proof First, we prove that $\frac{N+1}{2} \leq N - \alpha + 1 - \Phi((\rho - 1)\sqrt{\frac{s}{2}})(N - 2\alpha + 1)$. Moreover, let $H(s) = N - \alpha + 1 - \Phi((\rho - 1)\sqrt{\frac{s}{2}})(N - 2\alpha + 1)$. Then, we obtain $H'(s) = \frac{1-\rho}{4\sqrt{\pi s}} e^{-\frac{(\rho-1)^2 s^2}{8}} > 0$. Therefore, $H(s) > H(0) = \frac{N+1}{2}$ if $i < N - \alpha + 1 - \Phi((\rho - 1)\sqrt{\frac{s}{2}})(N - 2\alpha + 1)$. It follows that $N - \alpha + 1 - i > \Phi((\rho - 1)\sqrt{\frac{s}{2}})(N - 2\alpha + 1)$, that is, $\frac{N-\alpha+1-i}{N-2\alpha+1} > \Phi((\rho - 1)\sqrt{\frac{s}{2}})$. Because Φ is a monotonic function, we can obtain $\Phi^{-1}(\frac{N-\alpha+1-i}{N-2\alpha+1}) > (\rho - 1)\sqrt{\frac{s}{2}}$. Then $\Phi^{-1}(\frac{N-\alpha+1-i}{N-2\alpha+1})\sqrt{\frac{2}{s}} > \rho - 1$. Finally, we multiply both sides of the above equation by σ^2 and simplify it to obtain $\sigma_\rho^2 = \frac{\sigma^2 + \sqrt{\frac{2}{s}}\sigma^2\Phi^{-1}(\frac{N-\alpha+1-i}{N-2\alpha+1})}{\rho} > \sigma^2$. □

From Lemmas 3.1 and 3.2, we obtain the following corollary.

Corollary 3.3 Suppose the following condition is satisfied:

$$i_0 = N - \alpha + 1 - \Phi((\rho - 1)\sqrt{\frac{s}{2}})(N - 2\alpha + 1). \tag{17}$$

If $i \leq i_0$, then the following relationship holds:

$$\sigma_\rho^2 > \sigma^2. \tag{18}$$

We set $i = [i_0]$ and denote the corresponding result by σ_f^2 as follows:

$$\sigma_f^2 = \frac{\sigma^2 + \sqrt{\frac{2\sigma^4}{s}} \Phi^{-1}(\frac{N-\alpha+1-[i_0]}{N-2\alpha+1})}{\rho}, \tag{19}$$

From this, we obtain $\sigma_f^2 > \sigma^2$.

Using Corollaries 3.2 and 3.3, we establish the following theorem.

Theorem 4 If the conditions of Corollary 3.3 are satisfied, the noise level can be estimated as follows:

$$\hat{\sigma}^2 = \frac{d_1\sigma_f^2 + d_2\sigma_w^2}{d_1 + d_2}, \tag{20}$$

where

$$d_1 = -\Phi^{-1}\left(\frac{1 - \alpha}{N - 2\alpha + 1}\right)\sqrt{\frac{2}{s}}, \tag{21}$$

$$d_2 = \frac{(1 - \rho) + \Phi^{-1}(\frac{N-\alpha+1-[i_0]}{N-2\alpha+1})\sqrt{\frac{2}{s}}}{\rho}. \tag{22}$$

Proof From (14) and (19), we obtain the following equation:

$$\frac{\sigma^2 - \sigma_w^2}{\sigma_f^2 - \sigma^2} = \frac{-\Phi^{-1}\left(\frac{1-\alpha}{N-2\alpha+1}\right)\sqrt{\frac{2}{s}}\sigma^2}{\frac{(1-\rho)+\Phi^{-1}\left(\frac{N-\alpha+1-l(i_0)}{N-2\alpha+1}\right)\sqrt{\frac{2}{s}}\sigma^2}{\rho}} \tag{23}$$

Let $d_1 = -\Phi^{-1}\left(\frac{1-\alpha}{N-2\alpha+1}\right)\sqrt{\frac{2}{s}}$ and $d_2 = \frac{(1-\rho)+\Phi^{-1}\left(\frac{N-\alpha+1-l(i_0)}{N-2\alpha+1}\right)\sqrt{\frac{2}{s}}}{\rho}$. Then (23) becomes

$$\frac{\sigma^2 - \sigma_w^2}{\sigma_f^2 - \sigma^2} = \frac{d_1}{d_2} \tag{24}$$

Therefore, the precise noise level can be estimated by solving (24), that is, $\hat{\sigma}^2 = \frac{d_1\sigma_f^2 + d_2\sigma_w^2}{d_1 + d_2}$. □

3.2 Proposed algorithm

Once the initial flat patches have been selected, the eigenvalues of the covariance matrix of these patches can be obtained. In (3), σ_w^2 is the minimum eigenvalue. According to Theorem 3, σ_f^2 in (19) is the $[i_0]^{th}$ eigenvalue divided by ρ . Thus, the noise level can be calculated via (20). The selection of the initial flat patches depends on the actual noise level. Therefore, the flat patches and the noise level estimation result are constantly updated via an iterative process, which increases the accuracy of the final calculation. Based on the analysis that is described above, the proposed algorithm for noise level estimation can be described as follows.

Algorithm 1 Selecting the flat patches and estimating the noise variance

Require: Noisy image

Ensure: Noise level σ

1: Estimate the initial noise level σ_0 with $k = 0$

While the flat patches are unstable **do**

2: Calculate τ_{k+1} using (1) and select the weak textured patches V

3: For V , use Algorithm 1 in [23] to select the flat patches I

4: Calculate $\sum_{\mathbf{p}} \mathbf{p}$ using (2), where $\mathbf{p}_i \in I$

5: Calculate σ_w^2 using (3)

6: For all patches in I , calculate σ_f^2 using (19)

7: Calculate $\hat{\sigma}_{k+1}^2$ using (20)

8: $k = k + 1$

End while

return Noise level $\hat{\sigma}_{k+1}^2$.

In the proposed algorithm, the three parameters, σ_0 , δ , and w are configured. In the method that is suggested in [19], the initial noise level σ_0 is initially estimated from the minimum eigenvalue of the covariance matrix of all patches. Then, we only need to consider the remaining parameters, namely, δ and w . The value of parameter δ , which is a significance level, ranges from 0 to 1. Parameter w represents the patch size. To partition an image in a meaningful manner, the value of w should be neither too big nor too small. The selection of these two parameter values is important for the proposed algorithm. In Section 4.1, the parameter design procedure is described in detail.

4 Experimental analysis

In this section, the optimal parameters are determined by testing the proposed algorithm using the parameters in the training set, and the experimental results regarding the accuracy and robustness of the proposed algorithm are presented. We use the following four well-known image datasets, which are typically used to evaluate image noise level estimation methods: The first image dataset is comprised of 10 standard image processing test images from the IVC databases [4]: Avion, Barbara, Boats, Clown, Fruit, House, Isabe, Lena, Mandr, and Peppers. The resolution of these images is 512×512 . The second image dataset was obtained from the Tampere image dataset (TID2008) [23] and contains 25 images that of size 512×384 . The third image dataset is LIVE [27], which contains 29 images with various resolutions. The last image dataset is BSDS500 [3], which contains three image folders: BSDS500-test (200 images), BSDS500-train (200 images), and BSDS500-val (200 images); the resolution of these images is 481×321 . In our experiments, zero-mean Gaussian noise with the standard deviations of $\sigma = 5, 10, 15, 20, 25, 30, 40, 50, 60, 70, 80, 90$, and 100 is added to all the images in the datasets. Finally, state-of-the-art algorithms [5, 15, 19, 24, 34], whose source codes are available online^{1,2,3,4}, are compared with the proposed algorithm. The code of the proposed algorithm can be found online at <https://ww2.mathworks.cn/matlabcentral/fileexchange/64519-natural-image-noise-level-estimation-based-on-flat-patches-and-local-statistics>. All the methods are implemented in MATLAB (24 GB RAM, 2.66 GHz CPU, and an Intel(R) Xeon(R) processor).

4.1 Parameter configuration

Parameters δ and w are configured via trial and error. First, we determine the optimal value of w . In the interval $(0, 1)$, we use insertion points with a step-size of 0.1 as candidate values for δ and consider limiting w to a reasonable range. In [19], Liu et al. selected $w = 7$ as the patch size. In [24], the value of w was selected as $w = 5$ and w increased with the image size. In [15], Jiang et al. selected $w = 5$ and $\delta = 0.9$ as the optimal values and reported that their algorithm is more suitable for high-frequency images if δ is small. In most algorithms, the optimal patch size is set to a value that is between 5 and 9. Thus, we consider these values as candidate values. To enhance the adaptability of the algorithm to high-frequency images, we consider values that are smaller than 0.9; specifically, the values of 0.7, 0.8, and 0.9 are considered. Then, we introduce these parameters into the proposed algorithm and apply the proposed algorithm to noisy data that are simulated from 200 natural images in BSDS500-train [3]. Additionally, large-range synthetic Gaussian noise with the standard deviations of $\sigma = 5, 10, 15, 20, 25, 30, 40, 50, 60, 70, 80, 90$, and 100 is added to each clean image. To improve the accuracy of parameter selection, 50 simulations are conducted in each case and the average value is considered. Subsequently, we evaluate the accuracy and robustness of the proposed algorithm under various parameter values by using the evaluation matrix that is defined in Section 4.2. Figure 1 presents the results for various parameter values. According to Fig. 1a and b, among the values of δ that are considered in the experiments, the estimation

¹<http://physics.medma.uni-heidelberg.de/cms/projects/132-pcanle>

²<http://www.ok.sc.e.titech.ac.jp/res/NLE/AWGNestimation.html>

³<http://people.csail.mit.edu/danielzoran/>

⁴<http://appsrv.cse.cuhk.edu.hk/gychen/>

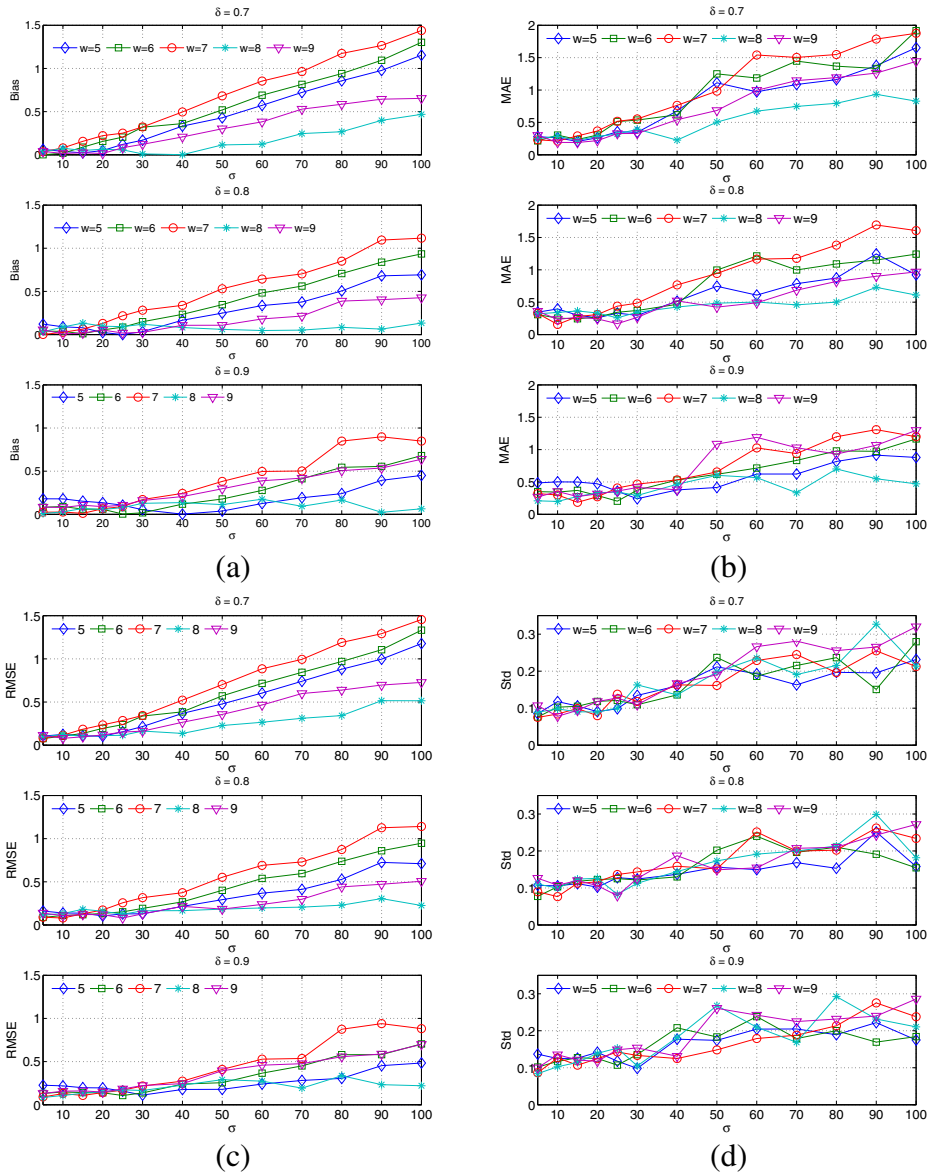


Fig. 1 Results of proposed algorithm with various values of parameters δ and w for DSDS500-train (200 images). **a** Bias, **b** MAE, **c** RMSE, and **d** Std

result is most accurate when $w = 8$ because the Bias value and the maximum absolute error (MAE) value are smaller in most cases. Next, we consider the overall performance. As shown in Fig. 1c, the root mean square error (RMSE) values that correspond to $w = 5, 6, 7,$ and 9 are larger than the RMSE value that corresponds to $w = 8$ with the same noise level. As shown in Fig. 1d, for all values of δ and w , the difference between the Std values is very small. However, a larger value of σ may lead to a larger Std value. Therefore, we determine

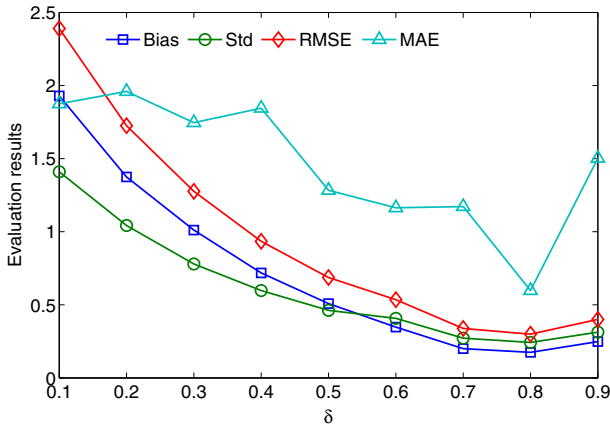


Fig. 2 Evaluation results of the proposed algorithm with respect to δ

8 to be the optimal value for parameter w . Next, optimal value of parameter δ is determined. We consider the initial value of δ to be 0.1 and increment it to the final value of 0.9 using a step-size of 0.1. The final result is obtained by utilized these values of δ and w in the proposed algorithm. The results are presented in Fig. 2. According to this figure, the Bias, Std, and RMSE values are smaller when $\delta = 0.8$. Therefore, we select $\delta = 0.8$ and $w = 8$ as the optimal parameter values.

4.2 Evaluation metrics

To evaluate the noise estimation performance, we use three well-established criteria, namely, accuracy, reliability and overall performance, which have been considered in most studies in the literature. Accuracy and reliability are typically represented by the average estimation error and the variance of the estimation errors, respectively. Thus, in this study, we employ the following four indicators to evaluate the performance of the proposed algorithm.

Estimation Bias is defined as follows:

$$Bias(\hat{\sigma}) = |\mathbb{E}(\sigma - \mathbb{E}(\hat{\sigma}))|. \tag{25}$$

The robustness of an estimator is defined as follows:

$$Std(\hat{\sigma}) = \sqrt{\mathbb{E}[\sigma - \mathbb{E}(\hat{\sigma})]^2}. \tag{26}$$

The *RMSE* is defined as follows:

$$RMSE(\hat{\sigma}) = \sqrt{Bias^2(\hat{\sigma}) + Std^2(\hat{\sigma})}. \tag{27}$$

The *MAE* is defined as follows:

$$MAE(\hat{\sigma}) = \max\{|\hat{\sigma}_1 - \sigma|, |\hat{\sigma}_2 - \sigma|, \dots, |\hat{\sigma}_M - \sigma|\}. \tag{28}$$

4.3 Results

4.3.1 Patch selection

According to (20), the estimation results are closely related to the number of flat patches. Therefore, accurate flat patch selection leads to accurate estimation results. Here, we compare the patch selection results of Algorithm 1 with those of various other algorithms. We chose four images from DSDS500-test, namely, #130066, #77062, #107072, and #108004, which are shown in the first row of Fig. 3. The second row presents the results that were obtained by the weak textured patch selection method that was reported in [19]. The third row presents the results that were obtained via the flat patch selection method that was reported in [15]. The last row presents the results that were obtained by the proposed algorithm. All selected patches are shown in white. In the first two images, the total number of patches that were selected by the algorithm that was reported in [15] exceeds the number of patches that were selected by the algorithm that was reported in [19]. For the last two images, the opposite is true. However, for all images, the flat patches that were selected by the proposed algorithm were closest to the actual flat area. According to Fig. 3, the patches that were used in the proposed algorithm approximated the actual flat area; hence, improved accuracy in flat patch selection was realized.

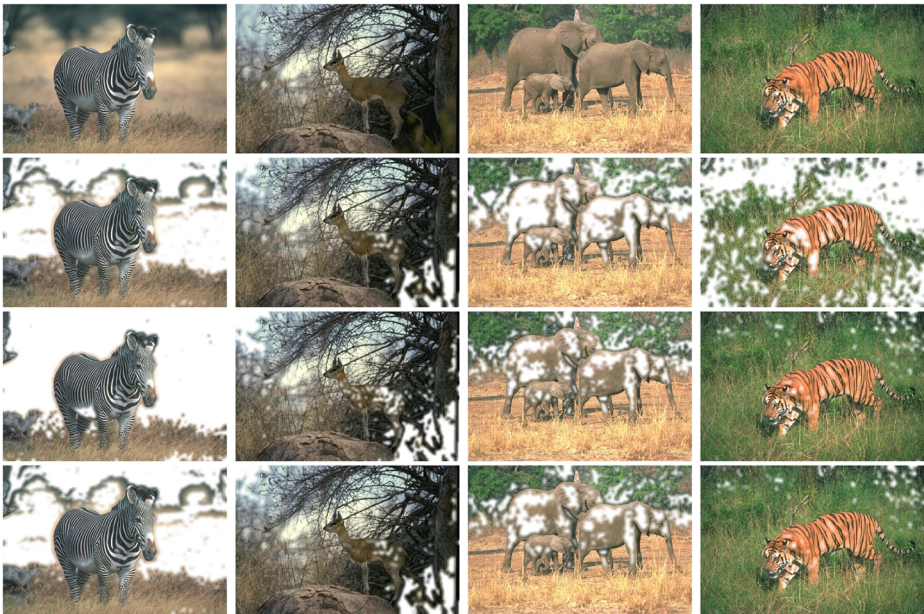


Fig. 3 Comparison of patch selection results, where the white regions represent the patches that were selected using various patch selection methods. The first row shows images #130066, #77062, #107072, and #108004 from BSDS500-test. The second row presents the results that were obtained by the weak textured patch selection method that was reported in [19]. The third row presents the results that were obtained by the flat patch selection method that was reported in [15]. The last row presents the results that were obtained by the proposed algorithm

Table 2 Results of the compared methods for BSDS500-test (200 images), where bold font indicates the best result for each noise level

σ	RMSE		Std									
	Ref. [34]	Ref. [19]	Ref. [24]	Ref. [15]	Ref. [5]	Ours	Ref. [34]	Ref. [19]	Ref. [24]	Ref. [15]	Ref. [5]	Ours
5	1.3460	0.1102	0.2467	0.1762	0.0496	0.1163	1.2913	0.1097	0.1891	0.1641	0.0412	0.1156
10	1.3662	0.1463	0.2009	0.2801	0.0609	0.1720	1.2706	0.1457	0.1217	0.2318	0.0543	0.1560
15	1.5147	0.1880	0.2332	0.3279	0.0885	0.2217	1.3842	0.1858	0.1795	0.2156	0.0657	0.1905
20	1.6067	0.1948	0.2795	0.3877	0.1377	0.2275	1.4417	0.1847	0.2594	0.2029	0.0980	0.1920
25	1.6055	0.2276	0.3373	0.4572	0.1717	0.2247	1.4440	0.1927	0.3373	0.2043	0.1109	0.1953
30	1.6036	0.2689	0.4317	0.5249	0.2029	0.2483	1.3907	0.2046	0.4148	0.2060	0.1322	0.2183
40	1.6798	0.3753	0.6979	0.6548	0.2633	0.2071	1.4189	0.2121	0.5305	0.2116	0.1721	0.1877
50	1.6806	0.5152	1.0902	0.7885	0.3374	0.2366	1.3996	0.2429	0.6839	0.2316	0.2171	0.2308
60	1.6346	0.6599	1.5299	0.9245	0.3626	0.2332	1.3511	0.2444	0.7583	0.2352	0.2445	0.2293
70	1.6051	0.8181	1.9939	1.0722	0.4902	0.2641	1.3377	0.2610	0.8042	0.2584	0.3561	0.2638
80	1.6102	0.9992	2.4399	1.1809	0.4956	0.2708	1.3474	0.2677	0.7905	0.2706	0.3274	0.2699
90	1.5721	1.1441	2.9029	1.3534	0.5612	0.2667	1.2903	0.2932	0.8436	0.2925	0.3792	0.2622
100	1.5231	1.3123	3.3957	1.4837	0.6127	0.2838	1.2958	0.3025	0.8119	0.3029	0.4302	0.2780

Table 2 (continued)

σ	Std												
	RMSE	Ref. [34]	Ref. [19]	Ref. [24]	Ref. [15]	Ref. [5]	Ours	Ref. [34]	Ref. [19]	Ref. [24]	Ref. [15]	Ref. [5]	Ours
		MAE											
	Bias												
5	0.3796	0.0107	0.1584	0.0642	0.0276	0.0123	6.4848	0.8326	2.2950	1.2182	0.2702	0.7054	
10	0.5021	0.0135	0.1599	0.1573	0.0276	0.0723	5.7855	1.2499	0.8071	2.4714	0.3543	1.3411	
15	0.6152	0.0289	0.1490	0.2470	0.0593	0.1133	7.8444	1.4480	0.8184	2.3249	0.3244	1.5304	
20	0.7091	0.0618	0.1040	0.3304	0.0968	0.1220	8.5375	0.9346	0.6967	1.6913	0.6907	1.4767	
25	0.7018	0.1211	0.0027	0.4090	0.1310	0.1112	5.9402	1.0271	0.9544	1.8072	0.5485	1.4044	
30	0.7984	0.1745	0.1198	0.4828	0.1539	0.1184	5.4005	1.0217	1.2888	1.8441	0.6940	1.4000	
40	0.8991	0.3096	0.4535	0.6196	0.1993	0.0875	4.8551	0.7971	1.7367	1.6050	1.0005	1.0998	
50	0.9303	0.4543	0.8491	0.7538	0.2583	0.0520	4.5165	0.9580	2.6289	1.9354	1.1325	1.0408	
60	0.9200	0.6130	1.3288	0.8941	0.2677	0.0427	4.6535	1.0954	2.8763	1.6267	1.0089	0.9656	
70	0.8871	0.7753	1.8245	1.0405	0.3370	0.0110	4.7899	1.4086	3.6808	1.9349	3.5022	1.2401	
80	0.8815	0.9627	2.3083	1.1495	0.3721	0.0230	4.6413	1.7415	4.0048	2.0064	1.7158	1.0785	
90	0.8982	1.1059	2.7776	1.3214	0.4137	0.0484	4.7291	1.8686	4.7299	2.1881	1.6900	0.8462	
100	0.8004	1.2769	3.2972	1.4525	0.4363	0.0570	4.7970	2.0568	5.2750	2.1363	2.0796	0.8983	

Table 3 Results of the compared methods for IVC, where bold font indicates the best result for each noise level

σ	RMSE		Std										
	Ref. [34]	Ours	Ref. [19]	Ref. [24]	Ref. [15]	Ref. [5]	Ours	Ref. [34]	Ref. [19]	Ref. [24]	Ref. [15]	Ref. [5]	Ours
5	0.4340	0.4799	0.4799	0.5900	0.4793	1.1037	0.4293	0.3602	0.2936	0.3151	0.2563	0.7946	0.2470
10	0.3805	0.3447	0.4309	0.4661	0.4309	0.6214	0.3180	0.3018	0.2632	0.2963	0.1920	0.4468	0.1895
15	0.6183	0.2645	0.4545	0.4270	0.4545	0.4709	0.2724	0.3845	0.2422	0.3216	0.1837	0.3306	0.1921
20	0.8146	0.2754	0.5180	0.3844	0.5180	0.4150	0.2928	0.5056	0.2754	0.3796	0.2529	0.2882	0.2630
25	0.9640	0.2614	0.5005	0.3098	0.5005	0.3302	0.1881	0.6336	0.2478	0.3083	0.1789	0.2564	0.1832
30	1.1091	0.3128	0.6595	0.3980	0.6595	0.3320	0.2567	0.8105	0.3008	0.3677	0.2360	0.2417	0.2435
40	1.3037	0.3543	0.8254	0.8243	0.8254	0.2916	0.2571	1.0697	0.3046	0.6397	0.2544	0.2444	0.2544
50	1.4628	0.4113	1.0080	1.0943	1.0080	0.2498	0.2175	1.2557	0.2517	0.5955	0.2231	0.1973	0.2158
60	1.5787	0.5138	1.2232	1.7021	1.2232	0.2818	0.2672	1.4450	0.2968	0.7174	0.2657	0.2814	0.2649
70	1.5038	0.6707	1.3515	2.0362	1.3515	0.1600	0.2737	1.3586	0.2593	0.6891	0.2795	0.1585	0.2711
80	1.4644	0.7988	1.5066	2.4858	1.5066	0.3686	0.2387	1.3347	0.2408	0.6187	0.2323	0.3212	0.2272
90	1.3768	0.9869	1.6462	2.9415	1.6462	0.2725	0.2922	1.2626	0.2517	0.7818	0.2657	0.2597	0.2591
100	1.9312	1.0778	1.8031	3.3421	1.8031	0.4954	0.2360	1.9290	0.1900	0.5851	0.1737	0.3947	0.1714

Table 3 (continued)

σ	RMSE		Std											
	Ref. [34]	Ours	Ref. [24]	Ref. [19]	Ref. [24]	Ref. [15]	Ref. [5]	Ours	Ref. [34]	Ref. [19]	Ref. [24]	Ref. [15]	Ref. [5]	Ours
	Bias													
5	0.2421	0.3796	0.4988	0.4051	0.7661	0.3511	0.9061	0.9458	1.0228	0.9064	2.8189	0.8319		
10	0.2318	0.2226	0.3598	0.3858	0.4319	0.2555	0.6533	0.7310	1.0010	0.7693	1.5928	0.5977		
15	0.4842	0.1063	0.2810	0.4157	0.3354	0.1932	1.0866	0.6714	1.1104	0.7395	1.1754	0.6045		
20	0.6386	0.0040	0.0603	0.4520	0.2987	0.1288	1.5845	0.6693	1.0424	1.0398	1.0338	0.7889		
25	0.7266	0.0834	0.0304	0.4674	0.2080	0.0428	2.0790	0.5570	0.8241	0.7989	0.9151	0.4483		
30	0.7570	0.0855	0.1522	0.6159	0.2277	0.0814	2.5296	0.7719	0.8921	1.2469	0.8316	0.7537		
40	0.7452	0.1811	0.5198	0.7853	0.1591	0.0371	3.2338	0.6408	1.2490	1.4619	0.7260	0.7166		
50	0.7504	0.3253	0.9181	0.9830	0.1532	0.0275	3.5811	0.5526	1.5506	1.6186	0.5808	0.6419		
60	0.6360	0.4194	1.5435	1.1940	0.0148	0.0350	3.7658	0.6790	2.3848	1.9463	0.4779	0.7845		
70	0.6446	0.6186	1.9161	1.3223	0.0216	0.0382	3.5128	0.8955	2.7229	1.9928	0.2787	0.6181		
80	0.6026	0.7617	2.4076	1.4886	0.1808	0.0731	3.3829	0.9530	3.1518	2.1375	1.0383	0.5627		
90	0.5489	0.9543	2.8357	1.6246	0.0827	0.1351	3.0814	1.4973	3.7451	2.0552	0.4620	0.7497		
100	0.0910	1.0609	3.2905	1.7947	0.2993	0.1623	4.4898	1.3746	4.1580	2.1205	0.6676	0.4643		

Table 4 Results of the compared methods for TID2008, where bold font indicates the best result obtained for each noise level

σ	Std													
	RMSE		Ref. [34]		Ref. [19]		Ref. [24]		Ref. [15]		Ref. [5]		Ours	
5	1.3855	0.1428	0.2367	0.2370	0.2007	0.1932	1.2586	0.0950	0.0944	0.1163	0.1755	0.1031		
10	1.5422	0.1240	0.1517	0.2747	0.0894	0.1957	1.5192	0.1213	0.0508	0.1656	0.0845	0.1512		
15	1.2077	0.1280	0.1907	0.3258	0.1119	0.1844	0.9910	0.1267	0.1452	0.1470	0.1119	0.1426		
20	1.3112	0.1352	0.2133	0.3878	0.0868	0.1552	1.0149	0.1113	0.2111	0.1280	0.0860	0.1162		
25	1.4222	0.1958	0.3545	0.4429	0.0810	0.1368	1.0469	0.1399	0.3468	0.1288	0.0630	0.1180		
30	1.5001	0.1922	0.4291	0.5440	0.1253	0.1366	1.0638	0.1079	0.4028	0.1337	0.1103	0.1115		
40	1.5761	0.3237	0.8415	0.7133	0.1487	0.1686	1.0679	0.1862	0.6393	0.1718	0.1106	0.1576		
50	1.6360	0.4659	1.1722	0.8563	0.2588	0.1706	1.0922	0.3047	0.6899	0.1935	0.1893	0.1695		
60	1.6102	0.6101	1.5846	1.0482	0.2282	0.1862	1.0629	0.4083	0.6940	0.1759	0.1940	0.1829		
70	1.5486	0.7675	1.9323	1.2116	0.3328	0.2810	1.0440	0.4629	0.8232	0.2695	0.2600	0.2810		
80	1.5626	0.8659	2.3442	1.3715	0.4478	0.2586	1.1248	0.4024	0.8510	0.2419	0.3816	0.2583		
90	1.4985	0.9431	2.9643	1.5897	0.3904	0.2666	1.1337	0.3758	1.0343	0.2501	0.3194	0.2650		
100	1.5421	1.1635	3.5052	1.6958	0.4345	0.3727	1.1501	0.4687	0.9730	0.3509	0.2895	0.3683		

Table 4 (continued)

σ	RMSE										Std									
	Ref. [34]	Ref. [19]	Ref. [24]	Ref. [15]	Ref. [5]	Ours	Ref. [34]	Ref. [19]	Ref. [24]	Ref. [15]	Ref. [5]	Ours	Ref. [34]	Ref. [19]	Ref. [24]	Ref. [15]	Ref. [5]	Ours		
	Bias										MAE									
5	0.5791	0.1066	0.2171	0.2065	0.0974	0.1633	4.0923	0.3378	0.4830	0.4843	0.9300	0.4289								
10	0.2654	0.0255	0.1430	0.2191	0.0291	0.1243	5.6103	0.4672	0.2602	0.9268	0.3703	0.7709								
15	0.6902	0.0180	0.1235	0.2907	0.0004	0.1169	2.4596	0.4042	0.3822	0.8489	0.4108	0.6635								
20	0.8301	0.0768	0.0308	0.3661	0.0114	0.1030	2.7107	0.3069	0.4707	0.7034	0.2279	0.4626								
25	0.9626	0.1371	0.0737	0.4237	0.0510	0.0691	2.9319	0.3452	0.7931	0.8685	0.1342	0.5356								
30	1.0577	0.1591	0.1481	0.5273	0.0594	0.0790	2.9735	0.3477	0.8703	0.7723	0.2530	0.3524								
40	1.1592	0.2648	0.5472	0.6923	0.0994	0.0597	2.8817	0.5389	1.4253	1.1635	0.2855	0.5608								
50	1.2180	0.3524	0.9478	0.8342	0.1765	0.0185	3.1055	0.8778	1.9005	1.3557	0.6431	0.5653								
60	1.2095	0.4533	1.4246	1.0334	0.1203	0.0348	3.3470	1.2711	2.4176	1.2975	0.5852	0.3268								
70	1.1439	0.6122	1.7481	1.1813	0.2077	0.0017	3.3191	1.2692	2.8392	1.8890	0.8037	0.7044								
80	1.0847	0.7667	2.1842	1.3500	0.2343	0.0120	3.6144	1.2442	3.5237	2.0174	1.4876	0.8196								
90	0.9799	0.8649	2.7780	1.5699	0.2244	0.0291	3.4408	1.3267	4.3132	2.1841	0.9537	0.8181								
100	1.0273	1.0649	3.3675	1.6591	0.3240	0.0572	4.0173	1.8392	4.5801	2.9589	1.0194	1.3725								

Table 5 Results of the compared methods for all datasets, where bold font indicates the best result

Method	RMSE	Std	Bias	MAE
Ref. [34]	1.5866	1.4378	0.6711	8.6720
Ref. [19]	0.6843	0.5258	0.4380	3.0462
Ref. [24]	1.7460	1.4180	1.0190	5.4100
Ref. [15]	0.9105	0.5541	0.7224	3.2398
Ref. [5]	0.3448	0.2933	0.1812	3.22962
Ours	0.2577	0.2498	0.0634	2.7288

4.3.2 Noise level estimation results

Using the parameter values that were selected in Section 4.1, we compare the proposed algorithm with state-of-the-art algorithms [5, 15, 19, 24, 34] on various scenes under various noise levels. For the algorithms that were reported in [5, 15, 19, 24], the parameter values that were reported in the original studies are used. For the algorithm that was reported in [34], the result is sensitive to the initial value. To ensure a fair comparison, we select the initial value of 0.5 and increment with a step-size of 0.5 until we obtain the optimal result. In the comparative experiments, the final noise level estimation result is obtained by averaging the noise level estimates of each channel when handling a color image in each image dataset.

First, we present the results that were obtained for the challenging BSDS500-test dataset. This dataset contains 200 images that depict scenes that closely resemble real-world environments. Most of the images in the dataset contain small homogenous areas and rich features. The proposed algorithm yields more accurate noise level estimation results, particularly when the added true noise level is high. According to Table 2, on low noise levels, the algorithm that was proposed in [5] and [19] outperforms the other methods. In contrast, the RMSE and Bias values of the proposed algorithm are smaller than those of the other schemes when the noise level exceeds 30. Hence, for the BSDS500-test dataset, the proposed algorithm is more accurate and scene-independent under higher noise levels.

Moreover, according to Table 3 on the IVC [4] dataset, the proposed algorithm outperforms the other algorithms. The RMSE demonstrates significant comparative advantages for almost all noise levels; hence, the proposed algorithm is more accurate and robust on the IVC dataset.

Next, we consider the estimation results that were obtained for the TID2008 dataset, which contains 25 RGB images without any compression and wherein one image is artificial while the other images depict real-world scenes. Although the images in this dataset are considered to be noise-free, they still contain low levels of noise, with the exception of the artificial image. By following the methodology that was proposed in [19, 24], we correct each estimation result by calculating $\sigma_{corr}^2 = \sigma_{est}^2 - \sigma_{ref}^2$, where σ_{ref}^2 represents the inherent noise that is contained in each reference image. These values are available online at <http://physics.medma.uni-heidelberg.de/cms/projects/132-pcanle>. Moreover, σ_{est}^2 represents the estimation results. According to Table 4, the RMSE, Bias, and MAE values of the proposed algorithm are smaller than those of the other schemes when the noise level is high. There is no significant difference between the Std value that is obtained by the algorithm and the minimum Std value; thus, the accuracy of the proposed algorithm is higher when the reliability is the same.

Finally, we apply the proposed algorithm to all images in the IVC, TID2008, LIVE, BSDS500-test, and BSDS500-val datasets. According to the results, which are presented in Table 5, the proposed approach yields the highest accuracy among all compared methods [5, 15, 19, 24, 34].

5 Conclusions and future work

In this paper, we have proposed a new patch-based algorithm that linearly combines overestimated and underestimated results to evaluate the noise levels in images that are contaminated by Gaussian noise. Moreover, we have discussed the relationship between the eigenvalues and the true noise level, which forms the theoretical foundation of the proposed algorithm. Our algorithm can overcome the underestimation of noise level estimation algorithms that employ the minimum eigenvalue. In comparison with five state-of-the-art noise level estimation algorithms, the proposed algorithm yields higher accuracy and robustness for a large range of visual content and noise conditions. The parameters were determined according to the experimental results that were obtained by the algorithm for the dataset. The selected parameters render the algorithm widely applicable, and the results obtained by the algorithm have excellent accuracy. However, the selected parameters may not be the optimal values. The optimal configuration of the algorithm's parameters will be the subject of future work.

Acknowledgments This study was supported by the National Natural Science Foundation of China (Grant no. 11671307, 61561019, 61763009 and 11761030), the Nature Science Foundation of Hubei Province (Grant no. 2015CFB262), and the Doctoral Scientific Fund Project of Hubei University for Nationalities (Grant no. MY2015B001). We would like to express our gratitude to the anonymous reviewers and editors for their valuable comments and suggestions, which led to the improvement of the original manuscript.

Publisher's note Springer Nature remains neutral with regard to jurisdictional claims in published maps and institutional affiliations.

References

1. Abdallah MB, Azar AT, Guedri H, Malek J, Belmabrouk H (2018) Noise-estimation-based anisotropic diffusion approach for retinal blood vessel segmentation. *Neural Comput Appl* 29(8):159–180
2. Aharon M, Elad M, Bruckstein A (2006) K-SVD: an algorithm for designing overcomplete dictionaries for sparse representation. *IEEE Trans Signal Process* 54(11):4311–4322
3. Arbeláez P, Maire M, Fowlkes C, Malik J (2011) Contour detection and hierarchical image segmentation. *IEEE Trans Pattern Anal Mach Intell* 33(5):898–916
4. Callet PL, Atrousseau F (2005) Subjective quality assessment irccyn/ivc database. <http://www.irccyn.ec-nantes.fr/ivcdb/>
5. Chen G, Zhu F, Heng PA (2015) An efficient statistical method for image noise level estimation. In: 2015 I.E. international conference on computer vision (ICCV), pp 477–485
6. Colom M, Lebrun M, Buades A, Morel JM (2015) A non-parametric approach for the estimation of intensity-frequency dependent noise. In: 2015 IEEE international conference on image processing, pp 4261–4265
7. Dabov K, Foi A, Katkovnik V, Egiazarian K (2007) Image denoising by sparse 3D transform-domain collaborative filtering. *IEEE Trans Image Process* 18(8):2080–2095

8. Dong W, Zhang L, Shi G, Wu X (2011) Image deblurring and super-resolution by adaptive sparse domain selection and adaptive regularization. *IEEE Trans Image Process* 20(7):1838–1857
9. Dong W, Zhang L, Shi G, Li X (2013) Nonlocally centralized sparse representation for image restoration. *IEEE Trans Image Process* 22(4):1620–1630
10. Donoho DL (1995) De-noising by soft-thresholding. *IEEE Trans Inf Theory* 41(3):613–627
11. Donoho DL, Johnstone IM (1995) Adapting to unknown smoothness via wavelet shrinkage. *Publ Am Stat Assoc* 90(432):1200–1224
12. Ghazi MM, Erdogan H (2016) Image noise level estimation based on higher-order statistics. *Multimed Tools Appl* 76(2):1–19
13. Hashemi M, Beheshti S (2010) Adaptive Noise Variance Estimation in BayesShrink. *IEEE Signal Process Lett* 17(1):12–15
14. Huang X, Chen L, Tian J, Zhang X, Fu X (2014) Blind noisy image quality assessment using block homogeneity. *Comput Electr Eng* 40(3):796–807
15. Jiang P, Zhang JZ (2016) Fast and reliable noise level estimation based on local statistic. *Pattern Recogn Lett* 78(C):8–13
16. Khmag A, Ramli AR, Al-Haddad SAR, Kamarudin N (2018) Natural image noise level estimation based on local statistics for blind noise reduction. *Vis Comput* 34(4):575–587
17. Kim DG, Shamsi ZH (2018) Enhanced residual noise estimation of low rank approximation for image denoising. *Neurocomputing* 293:1–11
18. Li D, Zhou J, Tang YY (2017) Noise Level Estimation for Natural Images Based on Scale-Invariant Kurtosis and Piecewise Stationarity. *IEEE Trans Image Process* 26(2):1017–1030
19. Liu X, Tanaka M, Okutomi M (2013) Single-image noise level estimation for blind denoising. *IEEE Trans Image Process* 2(12):5226–5237
20. Mandal S, Bhavsar A, Sao AK (2016) Noise adaptive super-resolution from single image via non-local mean and sparse representation. *Signal Process* 132:134–149
21. Olsen SI (1993) Estimation of noise in images: an evaluation. *Cvqip Graph Model Image Process* 55(4):319–323
22. Oyet AJ, Sutradhar B (2003) Testing variances in wavelet regression models. *Stat Probab Lett* 61(1):97–109
23. Ponomarenko P, Lukin V, Zelensky A, Egiazarian K, Carli M, Battisti F (2009) Tid2008-a database for evaluation of full-reference visual quality assessment metrics. *Adv Modern Radioelectron* 10(4):30–45
24. Pyatykh S, Hesser J, Zheng L (2013) Image noise level estimation by principal component analysis. *IEEE Trans Image Process* 22(2):687–699
25. Royston JP (1982) Algorithm as 177: Expected normal order statistics (exact and approximate). *J R Stat Soc* 31(2):161–165
26. Shapiro SS, Wilk MB (1972) An analysis of variance test for the exponential distribution (complete samples). *Technometrics* 14(2):355–370
27. Sheikh HR, Sabir MF, Bovik AC (2005) Live image quality assessment database release2. <http://live.ece.utexas.edu/research/quality>. Accessed 3 May 2017
28. Shi B, Pang ZF, Wu J (2015) Alternating split Bregman method for the bilaterally constrained image deblurring problem. *Appl Math Comput* 250:402–414
29. Shin DH, Park RH, Yang S, Jung JH (2005) Block-based noise estimation using adaptive Gaussian filtering. *IEEE Trans Consum Electron* 51(1):218–226
30. Witwit W, Zhao Y, Jenkins K, Addepalli S (2018) Global motion based video super-resolution reconstruction using discrete wavelet transform. *Multimedia Tools Appl* 77(20):27641–27660
31. Xie X, Wang C, Zhang A, Meng X (2014) A robust level set method based on local statistical information for noisy image segmentation. *Optik* 125(9):2199–2204
32. Xu S, Yang X, Jiang S (2017) A fast nonlocally centralized sparse representation algorithm for image denoising. *Signal Process* 131:99–112
33. Zhu X, Milanfar P (2010) Automatic parameter selection for denoising algorithms using a no-reference measure of image content. *IEEE Trans Image Process* 19(12):3116–3132
34. Zoran D, Weiss Y (2009) Scale invariance and noise in natural images. In: 2009 I.E. international conference on computer vision (ICCV), pp 2209–2216



Zhuang Fang received the B.S. degree from Hubei University for Nationalities, Enshi China, in 2003, and M.S. degree from Chongqing University, Chongqing, China in 2011. He is studying for a PHD at Wuhan University, Wuhan, China. He is currently a lecturer with School of Science, Hubei University for Nationalities, his research interests include image processing and mathematical modeling.



Xuming Yi received the B.S. degree in 1987 and Ph.D. degree in 1993 from Wuhan University. He is a professor at school of mathematics and statistics in Wuhan University. He has published over 50 research papers. His research interests include wavelet analysis and its application, digital signal processing, pattern recognition and machine learning.